Available online at www.sciencedirect.com
SCIENCE DIRECT
Journal of Solid State Chemistry 179 (2006) 2452–2457
JOURNAL OF SOLID STATE CHEMISTRY
www.elsevier.com/locate/jssc

# A one-step solvothermal route for the synthesis of nanocrystalline anatase $TiO_2$ doped with lanthanide ions

Daniele Falcomer[a], Matteo Daldosso[a], Carla Cannas[b], Anna Musinu[b], Barbara Lasio[c], Stefano Enzo[c], Adolfo Speghini[a,*], Marco Bettinelli[a]

[a]*Dipartimento Scientifico e Tecnologico, Università di Verona and INSTM, Ca' Vignal 1, Strada Le Grazie 15, I-37134 Verona, Italy*
[b]*Dipartimento di Scienze Chimiche, Università di Cagliari, SS 554 bivio per Sestu, 09042 Monserrato (CA), Italy*
[c]*Dipartimento di Chimica, Università di Sassari, via Vienna 2, I-07100 Sassari, Italy*

Received 6 February 2006; received in revised form 13 April 2006; accepted 30 April 2006
Available online 6 May 2006

**Abstract**

A one-step solvothermal synthesis is proposed for the preparation of nanocrystalline single-phase $TiO_2$ in the anatase form doped with lanthanide ions $Eu^{3+}$, $Er^{3+}$ and $Sm^{3+}$. The structural properties of these products have been investigated by using X-ray powder diffraction, electron microscopy and Raman spectroscopy. Furthermore, the laser-excited luminescence spectra of the samples have been measured and analyzed. Following this route, the doping process turns out to be highly favorite and the resulting materials show an efficient luminescence in the visible region.


*Keywords:* Solvothermal synthesis; $TiO_2$; Nanocrystalline; Lanthanide ions

## 1. Introduction

In recent years, a large and increasing number of studies has been devoted to titanium dioxide ($TiO_2$) [1] as this material is used in many technological applications and, particularly, in photocatalysis [2]. Concerning the two polymorphic forms rutile and anatase, it has been reported that the efficiency of $TiO_2$ as photocatalyst is higher when it is in the anatase form [1], even though the sample morphology plays a leading role in determining the photocatalytic activity. As a matter of fact, Degussa P-25 (a very fluffy mixture of anatase and rutile) is one of the most active catalyst for degradation of several organic dyes [3,4]. In addition, doping of the anatase $TiO_2$ phase with metal and rare-earth ions has been investigated with the two-fold aim of increasing the catalyst performance [5,6] and obtaining a material with optical properties exploitable in various technological applications such as optoelectronic devices and materials for illumination [7]. In order to produce these materials in the form of powders or thin films, the sol–gel synthesis route has been largely adopted, generally starting from precursors such as rare-earth nitrates and titanium alkoxides [5,8,9]. In alternative, the hydrothermal synthesis route has been used as an easy and rapid method to obtain single phase anatase $TiO_2$ [10–16]. However, while anatase can be successfully doped with transition metal ions [17], the hydrothermal approach shows inherent limitations for the synthesis of lanthanide doped anatase $TiO_2$. To overcome this difficulty, Jeon and Braun [15] proposed a hydrothermal synthesis of anatase doped with the $Er^{3+}$ ion by mixing the reagents in an autoclave reactor. Nevertheless, they used an opaque suspension due to early formation of erbium hydroxide in the strongly basic reaction environment. Owing to this, a biphasic mixture of precursors of lanthanide oxides and anatase in the obtained product could not be completely disregarded. However, with the present solvothermal synthesis, we wish to point out that it is possible to carry out the reaction in an autoclave starting from a fully homogeneous and transparent solution of lanthanide ions and titanium alkoxide, thus avoiding the formation of any

*Corresponding author. Fax: +39 045 802 7929.
*E-mail address:* adolfo.speghini@univr.it (A. Speghini).

0022-4596/$ - see front matter © 2006 Elsevier Inc. All rights reserved.
doi:10.1016/j.jssc.2006.04.043

starting suspension. In such a way, from a simultaneous precipitation of titanium and rare-earth hydroxides we expect to easily obtain a homogeneous dispersion of the $Eu^{3+}$, $Er^{3+}$ and $Sm^{3+}$ lanthanide ions in nanocrystalline $TiO_2$ in the anatase form.

The structural properties of powders prepared by the solvothermal approach have been investigated by using X-ray powder diffraction (XRPD), high resolution transmission electronic microscopy (HRTEM) and Raman spectroscopy while luminescence properties of the materials have been studied by using laser excited spectroscopy.

## 2. Experimental section

### 2.1. Sample preparation

The starting materials were titanium(IV) butoxide (Aldrich, 97%), $Eu(NO)_3 \cdot 5H_2O$ (Aldrich, 99.9%), $Er(NO)_3 \cdot 5H_2O$ (Aldrich, 99.9%), $Sm(NO)_3 \cdot 6H_2O$ (Aldrich, 99.9%), deionized $H_2O$, absolute ethanol and glacial acetic acid. In all cases, the nominal molar ratio between titanium and the lanthanide ion ($Eu^{3+}$, $Er^{3+}$ or $Sm^{3+}$) was 99:1, respectively. An undoped $TiO_2$ sample was also prepared as a reference using the same procedure. In a typical synthesis, 30 mL ethanol, 0.5 mL of acetic acid and 2 mL of deionized water containing the lanthanide nitrate were mixed under stirring. To this solution 5 mL of titanium(IV) butoxide were slowly added under vigorous stirring. After 15 min the still clear solution was introduced in a PTFE autoclave and heated at 150 °C at a heating rate of 100 K/h and kept at that temperature for 3 h. The corresponding pressure was about 10 bar. The obtained precipitate was filtered and dried at 110 °C for 2 h and then heat treated at 500 °C for 2 h. The europium concentration in the $TiO_2$:Eu sample was checked by inductively Coupled plasma analysis and it was found to be 0.84% with respect to titanium. Hereafter, the samples are denoted with $TiO_2$:Eu, $TiO_2$:Er and $TiO_2$:Sm.

### 2.2. X-ray powder diffraction and HRTEM

XRPD patterns were recorded overnight with a Bruker D8 diffractometer in the Bragg–Brentano geometry using Cu$K\alpha$ radiation ($\lambda = 1.5418$ Å). The X-ray generator worked at a power of 40 kV and 40 mA and the goniometer was equipped with a graphite monochromator in the diffracted beam. The resolution of the instrument (divergent and antiscatter slits of 0.5°) was determined using α-$SiO_2$ and α-$Al_2O_3$ standards free from the effect of reduced crystallite size and lattice defects. The powder patterns were analyzed according to the Rietveld method [18] using the program MAUD [19] running on a personal computer. It is worth to recall that the MAUD program takes into account precisely the instrument broadening and, under the selected assumption of isotropic peak broadening as a function of reciprocal space, performs the separation of the lattice strain contribution to the broadening from the reduced crystallite size. Relative agreement factors $R_{wp}$ and $R_B$ are generally reported to determine the ability of the implemented structural model in order to account for the experimental data, which are unavoidably affected by statistical noise due to the limited time of pattern collection.

HRTEM images were obtained with a JEM 2010 UHR, $LaB_6$ filament, working at 200 kV, equipped with a Gatan Imaging Filter and 794 slow scan CCD camera.

### 2.3. Raman and luminescence Spectroscopy

The 488.0 nm line of an Argon Laser (Stabilite 2017, Spectra-Physics) was used to excite the luminescence and Raman spectra. The emission radiation was collected by using an optical fiber and dispersed with a 0.46 m monochromator (HR460, Jobin-Yvon) equipped with a 150 lines/mm (for the luminescence spectra) or a 1200 lines/mm (for the Raman spectra) grating. An air cooled CCD device (Spectrum one, Jobin-Yvon) was employed to detect the emission radiation. All the spectroscopic measurements were performed at room temperature.

### 2.4. Infrared reflectance spectroscopy

The diffuse reflectance spectrum in the medium-infrared region (MIR) was measured at room temperature using a Nicolet Magna 760 FTIR spectrometer using an aluminated mirror as a reference.

## 3. Results and discussion

Fig. 1 shows the Raman spectrum of $TiO_2$:Eu sample, which appears to be representative also for those of $TiO_2$:Er and $TiO_2$:Sm samples. The Raman band centered at 516 $cm^{-1}$ (see Fig. 1) is ascribed to the $A_{1g}$ and a $B_{1g}$ vibrational modes of anatase $TiO_2$, while the band at 640 $cm^{-1}$ is attributed to an $E_g$ vibrational mode [20]. The Raman bands are broadened with respect to the data

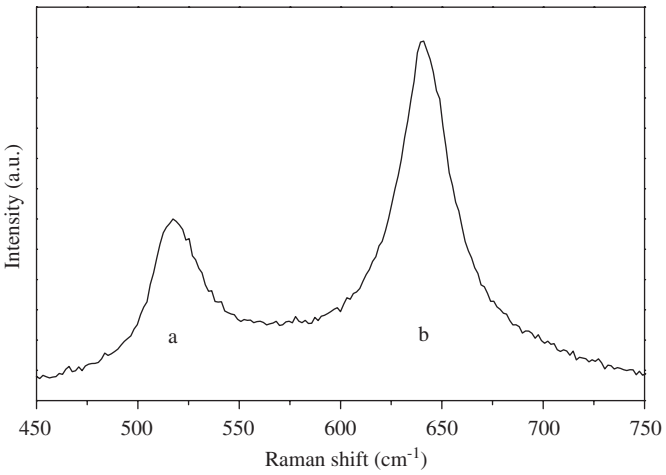


Fig. 1. Room temperature Raman spectrum of the nanocrystalline $TiO_2$:Eu sample.

reported in the literature [20], most probably due to the nanocrystalline size of the particles. In any case, a Raman band at 612 $cm^{-1}$, typical of the rutile $TiO_2$ phase [21], is not observed in the Raman spectrum, not even as a shoulder of the band centered at 640 $cm^{-1}$. This behavior is in agreement with the X-ray results (see below) which confirm that the samples under investigation are in pure anatase form.

Fig. 2 shows the XRPD spectra of $TiO_2$:Eu, $TiO_2$:Er and $TiO_2$:Sm as data points. As suggested by the Raman spectra, all samples are in pure anatase form (tetragonal geometry, space group no. 141 $I4_1/amd$) and the patterns

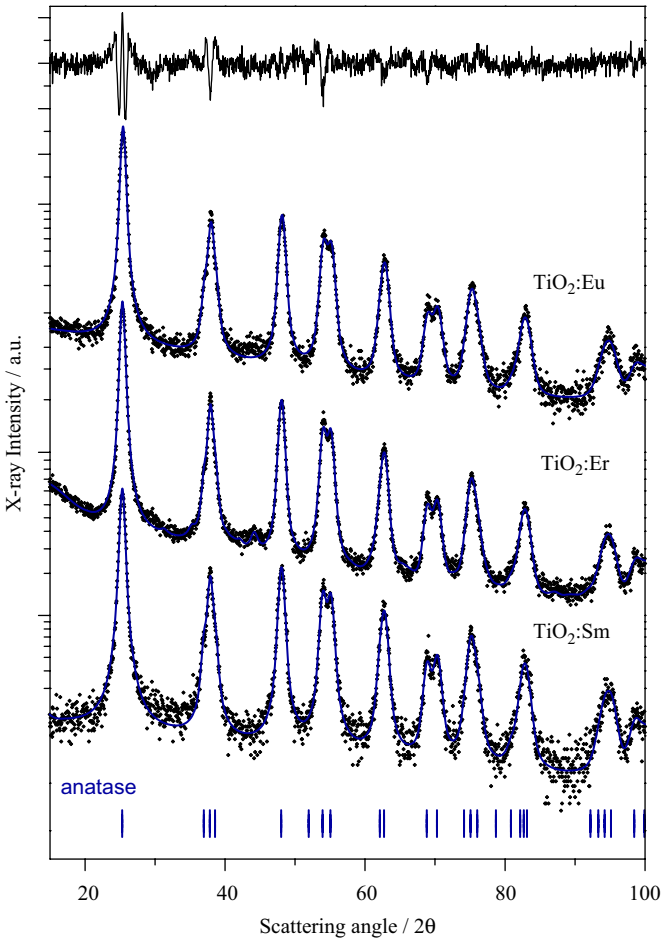


Fig. 2. XRPD experimental (dots) and Rietveld refined (solid lines) patterns of $TiO_2$:Eu, $TiO_2$:Er and $TiO_2$:Sm samples.

do not reveal any peak related to other phases of the Ti–O system such as rutile or brookite, neither lanthanide oxides. The X-ray peaks are very broadened due to the small mean coherent domain of diffraction and/or large lattice strain. The main structure and microstructure results of the Rietveld refinements (full lines) are reported in Table 1 for each sample. Higher agreement factors of Rietveld refinement are found for the $TiO_2$:Er sample, whose pattern appears more noisy (see Fig. 2).

It is worth noting that the unit cell volumes for the present doped $TiO_2$ samples are close to that of the undoped anatase sample (see Table 1) and to that reported in the literature for anatase $TiO_2$ [22]. Nonetheless, while the unit cell parameters of the doped specimens appear to be substantially the same, they are slightly different, beyond experimental uncertainty, with respect to those obtained for the present undoped anatase $TiO_2$ sample (see Table 1) and to those reported in the literature for anatase $TiO_2$ [22]. In addition, the axial ratio c/a for the doped samples is 2.509, to compare with the literature value of 2.514 [22]. The observed changes are ascribed to the presence of lanthanide ions in the $TiO_2$ host, with consequent strain and stress of the lattice.

The HRTEM images show a spherical morphology of the nanocrystals for all the samples. As an example, Fig. 3 shows the HRTEM image of the $TiO_2$:Eu sample, where the set of fringes corresponds to the [101] lattice planes of anatase phase.

The luminescence spectra of $TiO_2$:Eu, $TiO_2$:Er and $TiO_2$:Sm recorded at room temperature are shown in Fig. 4. All the samples exhibit an efficient laser excited luminescence although the brightness of $TiO_2$:Eu sample is about 10 time lower than that of reference red phosphor $YVO_4$:Eu (QHK63 produced by Phosphor Technology, England) measured in the same experimental conditions. The spectra consist of characteristic $Eu^{3+}$, $Er^{3+}$ and $Sm^{3+}$ emission bands due to *4f–4f* transitions as assigned in Fig. 4. The luminescence spectra of all the samples are characterized by inhomogeneously broadened bands typical of $Eu^{3+}$, $Er^{3+}$ and $Sm^{3+}$ ions in disordered environments, as already reported in the literature [8,9,17,23]. It is worth noting that in the anatase structure there is just one crystallographic titanium site 4(*a*) type of approximated octahedral geometry (point symmetry $D_{2d}$), with four "planar" Ti–O distances of 1.94 Å and two "axial" Ti–O distances of 1.98 Å. These two axial distances may be made

Table 1
Cell parameters, unit cell volume, axial ratio, crystallite size, lattice disorder, *Z* coordinate for 8(*e*) oxygen atoms and agreement factors of Rietveld refinement of XRPD data for $TiO_2$:Eu, $TiO_2$:Er, $TiO_2$:Sm and undoped $TiO_2$ specimens

| Sample | $a = b$ (Å) | $c$ (Å) | Unit cell volume (Å$^3$) | Axial ratio | crystallite size (nm) | Lattice disorder | $Z$ | $R_{wp}$ (%) | $R_b$ (%) |
|---|---|---|---|---|---|---|---|---|---|
| $TiO_2$:Eu | 3.7894(6) | 9.504(2) | 136.74(7) | 2.508 | 16(1) | 0.005(1) | 0.2081(15) | 9.9 | 9.4 |
| $TiO_2$:Er | 3.7872(5) | 9.502(2) | 136.30(6) | 2.509 | 16(2) | 0.004(1) | 0.2079(17) | 14.4 | 12.2 |
| $TiO_2$:Sm | 3.7875(5) | 9.499(1) | 136.27(6) | 2.508 | 17(2) | 0.004(1) | 0.2082(11) | 8.1 | 7.5 |
| $TiO_2$ | 3.784(5) | 9.512(1) | 136.20(6) | 2.514 | 30(3) | 0.002(1) | 0.2083(13) | 9.6 | 7.9 |
| $TiO_2$ [20] | 3.784 | 9.512 | 136.20 | 2.514 | — | — | — | — | — |

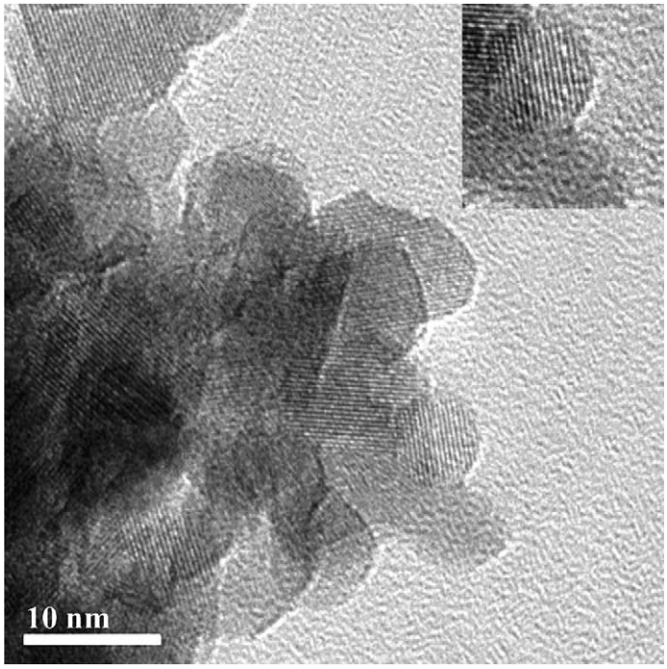


Fig. 3. HRTEM image of the nanocrystalline $TiO_2$:Eu sample. Inset: d-fringes (3.42 Å) corresponding to the [101] lattice planes of anatase $TiO_2$.

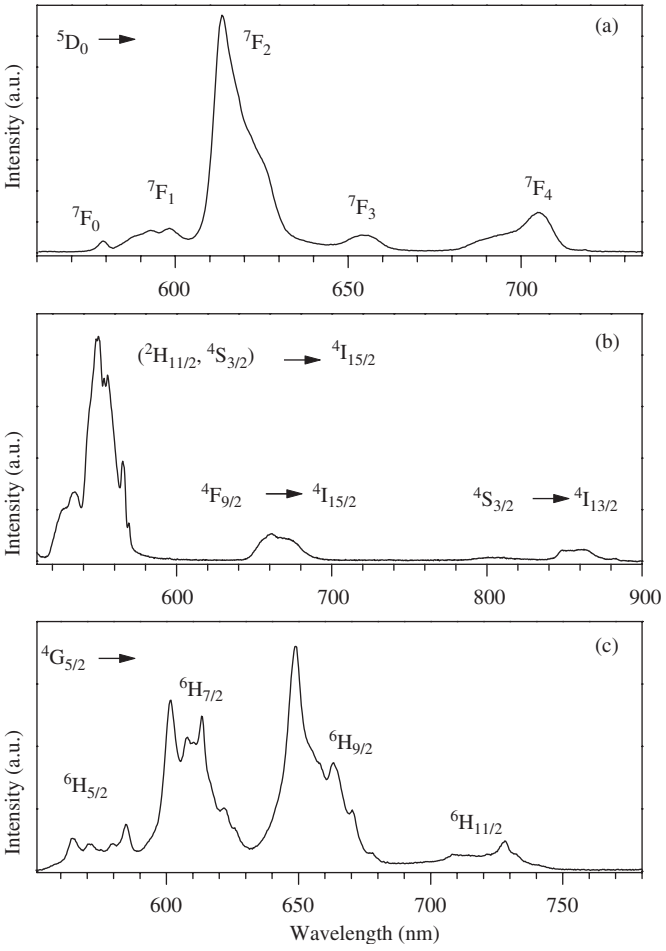


Fig. 4. Room temperature luminescence spectra of the nanocrystalline $TiO_2$:Eu (a), $TiO_2$:Er (b) and $TiO_2$:Sm (c) samples ($\lambda_{exc} = 488.0$ nm).

to coincide with the four planar distances by adjusting the $z$ coordinate of the 8($e$) oxygen atoms in the unit cell from the "equilibrium" figure 0.2083, substantially confirmed by our Rietveld refinement (see Table 1), to a new value of ca 0.2040. Thus, the observed broadening of laser-induced emission bands may be correlated to the high lattice disorder obtained from the XRPD data analysis (see Table 1). As a measure of this behavior, the FWHM of the $^5D_0 \rightarrow {}^7F_0$ emission band of the $Eu^{3+}$ ion is $93 \pm 2\,cm^{-1}$, confirming the high disorder of the crystalline environment of the $Eu^{3+}$ ions in the $TiO_2$ host. In fact, the FWHM value is similar to those found for lanthanide doped glass hosts [24]. The presence of such disorder is ascribed to the significant difference in the ionic radii in six-fold coordination for $Ti^{4+}$ (74.5 pm) and $Ln^{3+}$ (e.g. 108.7 pm for $Eu^{3+}$) (http://www.webelements.com/), so that the accommodation of the lanthanide ion cannot easily occur without distortions, which could be affected by a site-to-site variation. Moreover, the necessary charge compensation due to charge difference (3+ and 4+) could also occur in a variety of different ways, giving rise to a distribution of possible sites for the dopant ions.

It is well known that the asymmetry ratio

$$R = \frac{I(^5D_0 \rightarrow {}^7F_2)}{I(^5D_0 \rightarrow {}^7F_1)}$$

of the integrated intensities of the $^5D_0 \rightarrow {}^7F_2$ and $^5D_0 \rightarrow {}^7F_1$ transitions can be considered indicative of the asymmetry of the coordination polyhedron of the $Eu^{3+}$ ion [25]. In particular, the lower the $R$ value is, the higher is the site symmetry at the $Eu^{3+}$ ion. The value of the asymmetry parameter for the $TiO_2$:Eu sample, obtained from the measured emission spectra (see Fig. 4(a)) results to be $6.2 \pm 0.1$. This value appears to be lower than for $Eu^{3+}$ doped nanocrystalline $TiO_2$ powders prepared by a radio frequency thermal plasma oxidation technique ($R = 9.7$) [26]. However, the present value of $R$ does not agree with the relatively high symmetry of the $Ti^{4+}$ ions in the anatase structure ($D_{2d}$), as this symmetry is not compatible with a hypersensitive behavior of the $^5D_0 \rightarrow {}^7F_2$ transition [27]. This indicates that the $Eu^{3+}$ ion does not substitute for $Ti^{4+}$ without a significant site distortion.

We have subjected the three species to a high temperature annealing at 1500 °C. The XRD patterns, reported in Fig. 5, show that the main phase product is tetragonal rutile (space group $P4_2/mnm$, $a = 4.593(\pm 1)$ Å, $c = 2.959$ ($\pm 1$) Å), accompanied by a minor cubic phase identified as $Ln_2Ti_2O_7$ ($Ln$ = Eu, Er or Sm) (space group $Fd\bar{3}m$, $a$(Er) = 10.078($\pm 1$) Å [28], $a$(Eu) = 10.181($\pm 1$) Å [29], $a$(Sm) = 10.199($\pm 1$) Å [30], respectively). From the quantitative analysis of X-ray patterns reported in Fig. 5 it is possible to obtain the percentage of lanthanide with respect to titanium ions, that results to be 0.70 ($\pm 0.25$), 0.9 ($\pm 0.25$) and 1.1 ($\pm 0.25$) for $Eu^{3+}$, $Er^{3+}$ and $Sm^{3+}$, respectively. Moreover, the amount of the europium in the

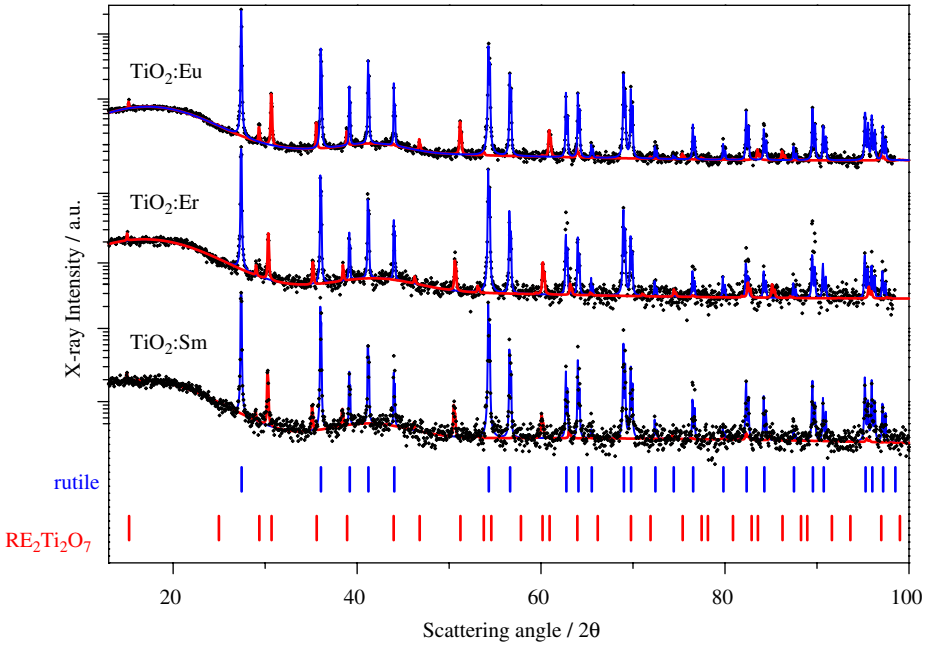


Fig. 5. XRPD experimental (dots) and Rietveld refined (lines) patterns of $TiO_2$:Eu, $TiO_2$:Er and $TiO_2$:Sm treated up to 1500 °C.

$TiO_2$:Eu sample was checked by Inductively coupled plasma analysis and found to be 0.84% with respect to titanium, very close to the nominal composition and in agreement with high-temperature XRD analysis.

These important results show that with our solvothermal synthesis it is possible to obtain lanthanide doped $TiO_2$ anatase and to control the dopant percentage without any significant loss of material, starting from homogeneous solutions at a selected working temperature and pressure.

## 4. Conclusion

The solvothermal synthesis approach can be successfully adopted to prepare nanocrystalline lanthanide doped single phase $TiO_2$ in the anatase form. The starting mixture was a fully homogenous solution similar to the one used in the sol–gel route. All obtained samples are formed by spherical nanoparticles with average diameter of 16 nm and the doping process can be easily achieved without significant loss of dopants. Moreover, the combined analysis of luminescence spectra and crystallographic results point out that the lanthanide ions replace titanium of the anatase matrix in a distorted and disordered octahedral local environment.

## Acknowledgments

The authors gratefully thank Gerry Sorce (Phosphor Technology, Hertfordshire, UK) for providing us the $YVO_4$:Eu (QHK63) sample. This work is part of a project co-financed by Fondazione Cariverona, Verona, Italy.

## References

[1] U. Diebold, Surf. Sci. Rep. 48 (2003) 53.
[2] O. Carp, C.L. Huisman, A. Reller, Prog. Solid State Chem. 32 (2004) 33.
[3] R.R. Bacsa, J. Kiwi, Appl. Catal. B 16 (1998) 19.
[4] H. Lachheb, E. Puzenat, A. Houas, M. Ksibi, E. Elaloui, G. Guillard, J.-M. Herrmann, Appl. Catal. B: Env. 39 (2002) 75.
[5] A.-W. Xu, Y. Gao, H.-Q. Liu, J. Catal. 207 (2002) 151.
[6] J. Liqiang, S. Xiaojun, X. Baifu, W. Baiqi, C. Weimin, F. Honggang, J. Solid State Chem. 177 (2004) 3375.
[7] G. Blasse, B.C. Grabmaier (Eds.), Luminescent Materials, Springer, Berlin, 1994.
[8] K.L. Frindell, M.H. Bartl, M.R. Robinson, G.C. Bazan, A. Popitsch, G.D. Stucky, J. Solid State Chem. 172 (2003) 81.
[9] A. Conde-Gallardo, M. Garcia-Rocha, I. Hernández-Calderón, R. Palomino-Merino, Appl. Phys. Lett. 78 (2001) 3436.
[10] M. Inagaki, Y. Nakazawa, M. Hirano, Y. Kobayashi, M. Toyoda, Int. J. Inorg. Mater. 3 (2001) 809.
[11] Y.V. Kolen'ko, V.D. Maximov, A.V. Garshev, P.E. Meskin, N.N. Oleynikov, B.R. Churagulov, Chem. Phys. Lett. 388 (2004) 411.
[12] Y.V. Kolen'ko, A.A. Burukhin, B.R. Churagulov, N.N. Oleynikov, Mater. Lett. 57 (2003) 1124.
[13] J. Ovenstone, K. Yanagisawa, Chem. Mater. 11 (1999) 2270.
[14] C.H. Cho, M.H. Han, D.H. Kim, D.K. Kim, Mater. Chem. Phys. 92 (2005) 104.
[15] S. Jeon, P.V. Braun, Chem. Mater. 15 (2003) 1256.
[16] S.D. Burnside, V. Shklover, C. Barbé, P. Comte, F. Arendse, K. Brooks, M. Grätzel, Chem. Mater. 10 (1998) 2419.
[17] M. Hirano, K. Date, J. Am. Ceram. Soc. 88 (2005) 2604.
[18] R.A. Young (Ed.), The Rietveld Method, University Press, Oxford, UK, 1993.
[19] L. Lutterotti, S. Gialanella, Acta Mater. 46 (1998) 101.
[20] T. Ohsaka, F. Izumi, Y. Fujiki, J. Raman Spectrosc. 7 (1978) 321.
[21] S.P.S. Porto, P.A. Fleury, T.D. Damen, Phys. Rev. 154 (1967) 522.
[22] PDF card no. 84–1285 related to ICSD # 202242.
[23] J. Ovenstone, P.J. Titler, R. Withnall, J. Silver, J. Phys. Chem. B 105 (2001) 7170.

[24] M. Wachtler, A. Speghini, K. Gatterer, H.P. Fritzer, D. Ajò, M. Bettinelli, J. Am. Ceram. Soc. 81 (1998) 2045.
[25] E.W.J.L. Oomen, A.M.A. van Dongen, J. Non-Cryst. Solids 111 (1989) 205.
[26] J.-G. Li, X. Wang, K. Watanabe, T. Ishigaki, J. Phys. Chem. B 110 (2006) 1121.
[27] R.D. Peacock, Struct. Bonding 22 (1975) 83.
[28] PDF card no. 73–1700.
[29] PDF card no. 23–1072.
[30] PDF card no. 73–1699.